RSC Advances

PAPER

View Article Online
View Journal | View Issue

Cite this: *RSC Adv.*, 2022, **12**, 31608

An optical strategy for detecting hypochlorite *in vitro* and cells with high selectivity and stability based on a lanthanide-doped upconversion probe†

Yuting Liu,[ab] Shiping Zhan,*[ab] Xin Su,[ab] Guozheng Nie,*[ab] Xiaofeng Wu*[c] and Yunxin Liu[ab]

The excessive use of sodium hypochlorite disinfectant for preventing COVID-19 can be harmful to the water environment and humans. More importantly, owing to hypochlorite being a biomarker of immune responses in living organisms, its abnormal production can damage nucleic acids and protein molecules, eventually causing many diseases (even cancer). Exploring a reliable, rapid, and non-invasive method to monitor the hypochlorite level *in vitro* and in cells can be significant. Herein, we report a novel ratiometric fluorescence sensing strategy based on Astrazon Brilliant Red 4G dye-sensitized $NaGdF_4$:Yb^{3+}, Er^{3+}@$NaYF_4$ core–shell upconversion nanoparticles (UCNPs@ABR 4G). Based on the combination mechanism of the fluorescent resonant energy transfer effect (FRET) and redox, a linear model of fluorescence intensity ratio and hypochlorite concentration was constructed for a fast response and high selectivity monitoring of hypochlorite *in vitro* and *in vivo*. The detection limit was calculated to be 0.39 μM. In addition, this sensing strategy possessed good stability and circularity, making it valuable both for the quantitative detection of hypochlorite in water and for the visualization of intracellular hypochlorite. The proposed optical probe is promising for the efficient and stable non-invasive detection of hypochlorite.

Received 29th August 2022
Accepted 24th October 2022

DOI: 10.1039/d2ra05414k

rsc.li/rsc-advances

1. Introduction

Since the outbreak of the Coronavirus Disease 2019 (COVID-19) began, great effort was made to disinfect public places.[1,2] Sodium hypochlorite (NaOCl) can produce hypochlorous acid (HClO) and hypochlorite (ClO^-) in water for disinfection and sterilization.[3–5] However, the excessive use of sodium hypochlorite can be hazardous to humans and the environment. Therefore, detecting the hypochlorite concentration in the water environment became a topic of significant current interest. Moreover, hypochlorite as a biomarker of active oxidation and biological immune response, plays an important role in disease resistance.[6–9] Nevertheless, the excessive or misplaced production of hypochlorite will damage some vital proteins and nucleic acids in the organisms, which can worsen some cardiovascular diseases and even cause cancer.[10–13] It is essential to explore a reliable, fast, efficient, and non-invasive hypochlorite detection method.

In the past few decades, researchers paid great attention on developing the detection strategies of hypochlorite, such as chromatography, colorimetric, spectrophotometry, electroanalytical, and fluorescence.[14–23] Compared with the other approaches, the fluorescence probe has a unique advantage for real-time detection *in situ*. However, some challenges still exist for most fluorescent strategies. For one thing, the commonly used fluorescence probe was an organic molecule, which possessed the shortcomings of complex preparation, low stability, and some difficulties in recycling. Secondly, some probes have a large bandwidth and substantial background interference. In addition, they often use high-energy UV or visible light as the excitation source, and will inevitably harm healthy cells and organs, which made them inapplicable for measuring analytes *in vivo*.[24–26] Although scientists developed some fluorescent probes in the near-infrared range of 700–900 nm in previous studies,[27–29] the limitations of a small Stokes shift, broadband fluorescence emission, and low signal-to-noise ratio still restrict its application. Therefore, exploring an efficient and stable inorganic fluorescence probe with a large Stokes shift and near-infrared (corresponding to the biological transparent window) excitation may be the key to achieving the high-performance detection of hypochlorite. As a vital fluorescent probe, rare-earth doped upconversion nanoparticles

[a]School of Physics and Electronic Science, Hunan University of Science and Technology, Xiangtan 411201, China. E-mail: spzhan86@163.com; gzhnie@hnust.edu.cn
[b]Hunan Province Key Laboratory of Intelligent Sensors and Advanced Sensor Materials, Xiangtan 411201, China
[c]School of Mechatronic Engineering and Automation, Foshan University, Foshan 528000, China. E-mail: xfwuvip@126.com

† Electronic supplementary information (ESI) available. See DOI: https://doi.org/10.1039/d2ra05414k

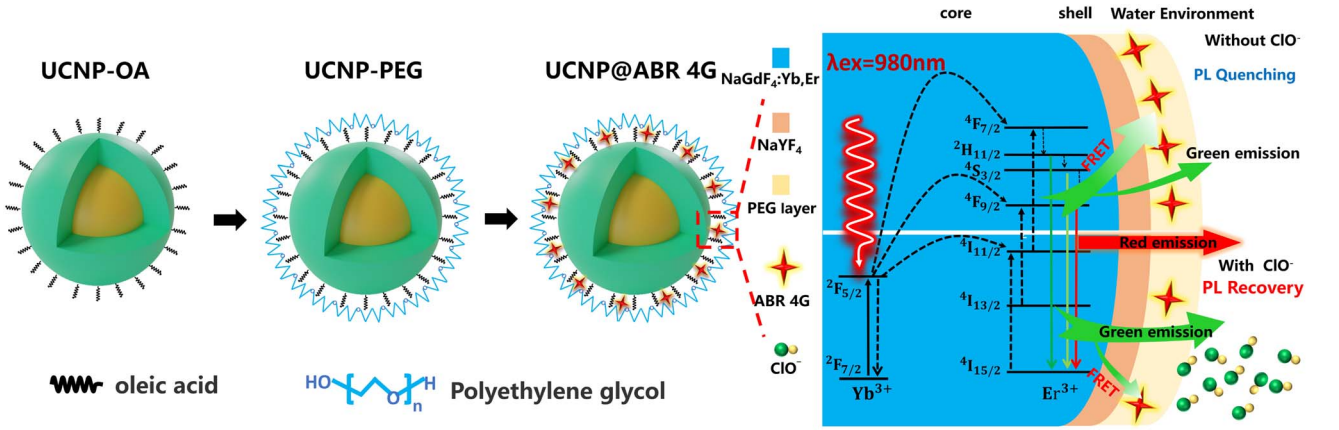

Fig. 1 Schematic illustration of ClO^- detection by using ABR 4G modified $NaGdF_4$: Yb^{3+}, Er^{3+}@$NaYF_4$ UCNPs.

(UCNPs) have the advantages of a large anti-Stokes shift, stable physicochemical properties, narrowband fluorescence emission, no background interference, abundant spectral lines, good water-solubility, high QY, and high penetration depth when compared with quantum dots, organic polymers, and fluorescent proteins.[30–32] UCNP fluorescent probes are suitable for the localization and real-time tracking of biomolecules and drug releases in living organisms by imaging techniques.[33–35] With the advantages of high sensitivity, fast response, and *in situ* detection, it has become a critical method for detecting and analyzing biomolecules in the biomedical field in recent years.

In this work, we propose a novel detection strategy that uses the UCNPs@ABR 4G fluorescent probe for detecting and imaging hypochlorite in aqueous solution and cells. The sensing mechanism is shown in Fig. 1. ABR 4G on the UCNP surface serves as the green emission quencher in this strategy. The quenched green emission can be gradually recovered with the existence of hypochlorite, which quantitatively monitors the hypochlorite level. The UCNPs@ABR 4G fluorescent probe also had high selectivity and sensitivity towards hypochlorite, and was further used for visual imaging in living onion epidermal cells. This method is a promising strategy for efficient and stable non-invasive hypochlorite detection both in water and in cells.

2. Experimental

2.1. Reagents

Rare-earth oxides (Gd_2O_3, Yb_2O_3, Er_2O_3, Y_2O_3), oleic acid (OA), octadecene (ODE, 90%), NaOH (98%), NH_4F (98%), cyclohexane, hydrochloric acid, polyethylene glycol (PEG), $BaCl_2 \cdot 2H_2O$ (99.5%), $MgCl_2 \cdot 6H_2O$ (98%), $CuCl_2 \cdot 2H_2O$ (99%), $CaCl_2$ (96%), $ZnCl_2$ (98%), $FeCl_3 \cdot 6H_2O$ (99%), $Na_2CO_3 \cdot 10H_2O$ (99%), $Na_2PO_4 \cdot 12H_2O$ (98%), $NaNO_2$ (99%), and H_2O_2 (30%) were purchased from Chemical Reagent Co., Ltd (Tianjin, P. R. China). ABR 4G was obtained from BioDuly Chemical Reagent Co., Ltd (Nanjing, P. R. China). Sodium hypochlorite (available chlorine 10%) was purchased from Huihong Chemical Reagent Co., Ltd (Hunan, P. R. China). The other commonly used solvents were purchased from Chemical Reagent Co., Ltd (Tianjin, P. R. China). All reagents were used as received without further purification.

2.2. Synthesis of $NaGdF_4$:Yb^{3+}, Er^{3+}@$NaYF_4$ core@shell UCNPs

The bare core $NaGdF_4$:Yb^{3+}, Er^{3+} and $NaGdF_4$:Yb^{3+}, Er^{3+}@$NaYF_4$ core–shell upconversion nanoparticles were synthesized by the method reported in the previous works.[36–40] The rare-earth chloride aqueous solution was prepared by dissolving rare-earth chloride in deionized water. The prepared aqueous solution of $LnCl_3$ ($LnCl_3$ = 80% Gd, 18% Yb, 2% Er), 2 mL OA and 2 mL ODE were added to a 50 mL flask A and heated to 180 °C. The solution was kept under nitrogen protection for 80 min, and the reaction system was converted into a transparent liquid. When the temperature cooled down to 60 °C, a methanolic solution of NaOH and NH_4F was added and stirred continuously for 30 min at 60 °C. For the other solution, the prepared YCl_3 aqueous solution, 2 mL OA, and 2 mL ODE were added to the 50 mL flask B, and the reaction conditions were the same, except that the rare-earth chloride solution in the flask was different. Under nitrogen protection, the reaction temperature of flask A was raised to 300 °C and kept for 80 min to form $NaGdF_4$:Yb^{3+}, Er^{3+} core nanoparticles. The shell precursor (flask B solution) was then mechanically pumped into flask A, and the reaction was continued for 30 min to obtain the $NaGdF_4$:Yb^{3+}, Er^{3+}@$NaYF_4$ hexagonal-phase core @ shell UCNPs.

2.3. Synthesis of $NaGdF_4$:Yb^{3+}, Er^{3+}@$NaYF_4$ core@shell UCNPs with PEG

A typical approach to obtaining aqueous dispersible upconverting lanthanide-doped $NaGdF_4$: 18% Yb^{3+}, 2% Er^{3+}@$NaYF_4$ core–shell nanoparticles. Firstly, a cyclohexane solution of upconversion nanoparticles with oleic acid ligand was centrifuged at 6000 rpm for 5 min. It was then dispersed in 30 mL diluted hydrochloric acid aqueous solution with a pH value of 4 and stirred at room temperature for 4 h. The precipitate was collected by centrifugation at 10 000 rpm for 15 min. Secondly, the collected nanoparticles were redispersed in a 5 mL aqueous

solution containing 0.5 mL PEG, stirred overnight, and separated from the precipitate. Finally, the collected nanoparticles were washed several times with ethanol and deionized water, and readily dissolved in water for later use.

2.4. Instrumentation

Transmission electron microscopy (TEM) measurements were obtained on a HF-5000 transmission electron microscope at an acceleration voltage of 80 kV, and the high-resolution transmission electron microscopy (HR-TEM) measurements were obtained on a JEM 3010 transmission electron microscope at an acceleration voltage of 200 kV. Upconversion fluorescence spectra were measured from 400 to 700 nm using a spectrometer (Hitachi F-2700) equipped with a power-adjustable 980 nm laser as the excitation source. The UV-vis absorption spectra were measured by a Hitachi F-4500 spectrometer.

Imaging of the onion epidermal cells incubated with nanoparticles was taken by an Olympus BX43 fluorescence microscope under the excitation of a NIR 980 nm laser. The multicolor fluorescence was obtained by a Tucsen H-694CICE digital camera. All of the measurements were performed at room temperature unless otherwise noted.

3. Results and discussion

We have designed a composite fluorescent probe UCNPs@ABR 4G for detecting the hypochlorite concentration in water and plant cells. Due to the FRET effect between the UCNPs and ABR 4G dye, which is discussed in detail in Section 3.2, the green emission of UCNPs will be dramatically quenched. However, as the hypochlorite is added, the redox reaction will decrease the amount of ABR 4G and therefore recover the emission again, as shown in Fig. 1. According to the intensity variation of the fluorescent signals, we constructed a linear model of IIRGRE (the integral intensity ratio of green to red emission) and the hypochlorite analyte concentration under the 980 nm excitation in water. In addition, the proposed fluorescent probe was used to visually monitor the hypochlorite at the cellular level.

3.1. Characterization of nanoparticles

The morphology of the synthesized $NaGdF_4$:Yb^{3+}, Er^{3+}@$NaYF_4$ nanoparticles were characterized by TEM and high-resolution TEM images, as shown in Fig. 2a and b. The distinct core/shell configuration and uniform particle size with an average diameter of 34 ± 3 nm (Fig. 2c) of the upconversion nanoparticles can be found. The lattice constant of the crystal faces (1010) was about 0.51 nm (Fig. 2b). The epitaxial shell layer can repair the surface defect of the active core and enhance the emission signal intensity by several folds, which will improve the signal-to-noise ratio and benefit the measurement during the application.

3.2. FRET mechanism between ABR 4G and UCNPs

FRET, as an important sensing strategy, usually occurs when a fluorescent donor and acceptor are efficiently coupled. FRET is an energy transfer phenomenon that occurs between two fluorescent molecules that are close to each other. When the donor's emission spectrum overlaps with the absorption band of the acceptor and the distance between the two molecules is within 10 nm, a non-radioactive energy transfer occurs from the donor to the acceptor, which is known as the FRET effect.[41–43] Here, for the fluorescent dye ABR 4G-modified UCNPs in our research, the UCNPs act as the energy donor, while the fluorescent dye molecular attached on its surface acts as the energy acceptor. According to the surface treatment, the ABR 4G can be very close to the UCNPs, which is quite helpful to the FRET process between them. This was attributed to the band overlap between the emission spectra of UCNPs and the absorption band of the ABR 4G molecule, as shown in Fig. 2d. Because of this band overlap, the green emission of $NaGdF_4$:Yb^{3+}, Er^{3+}@$NaYF_4$ UCNPs will be dramatically quenched when the ABR 4G is attached. As a result, a fluorescent probe was prepared based on the FRET effect by using UCNPs as the energy donor and the surface-modified dye as the energy acceptor. Here, the synthesized core–shell UCNPs showed three main emission bands centered at 520 nm, 540 nm and 655 nm under the excitation of 980 nm infrared laser (Fig. 2d), which are related to the electron

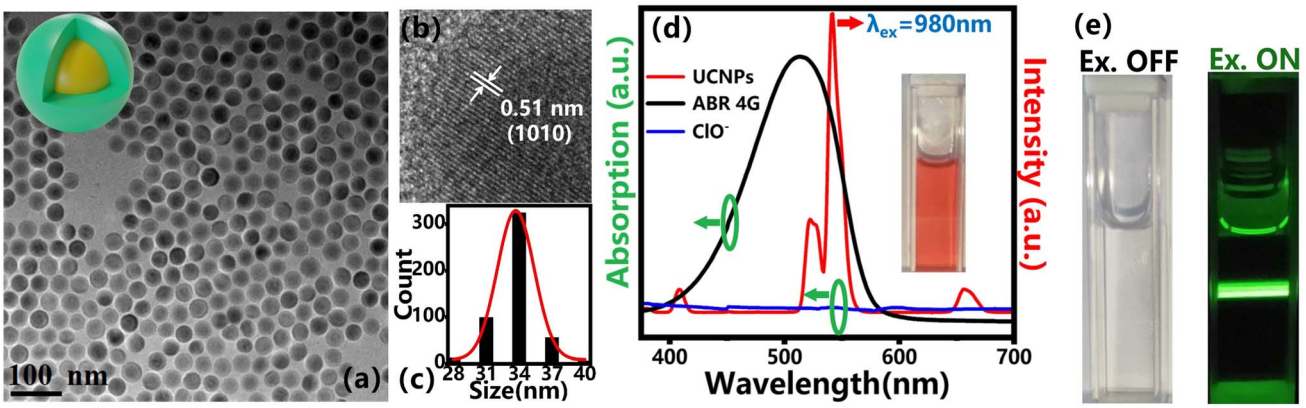

Fig. 2 (a) TEM and (b) HRTEM images of the $NaGdF_4$:Yb^{3+},Er^{3+}@$NaYF_4$ core–shell nanoparticles; (c) particle size distribution curve by DLS method; (d) the fluorescence intensity UCNPs, absorption of ClO^- and ABR 4G, inset: image of UCNPs@ABR 4G; (e) UCNPs dispersed in water with/without the excitation of the 980 nm laser.

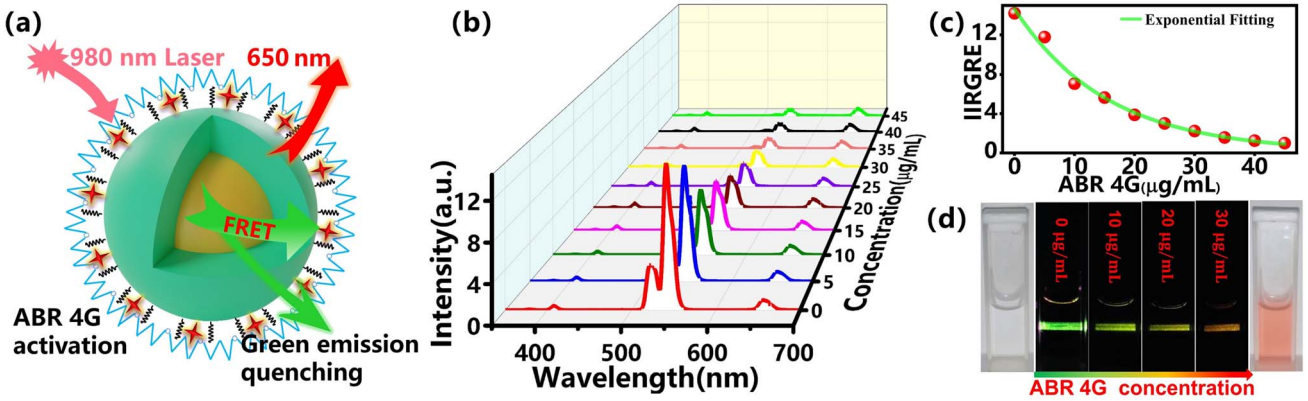

Fig. 3 (a) Diagram of the FRET mechanism between ABR 4G and UCNPs; (b) the fluorescence spectrum of the surface-modified UCNPs in the water under 980 nm near-infrared laser; (c) the dye concentration and the integral strength ratio; (d) fluorescence images of the emission quenching process.

transitions from the energy levels $^4H_{11/2}$, $^4S_{3/2}$, and $^4F_{9/2}$ to $^4I_{15/2}$ (Fig. 1), respectively. Since the green emission intensity was much stronger than the other emission bands, a bright green color can be observed when excited by NIR (shown in Fig. 2e). According to the optical properties in Fig. 2d, the emission band of Er^{3+} overlapped with the absorption band of ABR 4G from 510 to 570 nm, which will dramatically quench the green emission of the UCNPs when their surfaces were modified by the fluorescent dye. For a clear illustration of the sensing mechanism, the absorption of ClO^- was also measured. The nearly flat and low absorption spectra revealed that there would be no direct interaction between the bare UCNPs and ClO^-.

We firstly focused on the relation between the fluorescent dyes and UCNPs. Here, the UCNPs were modified by ABR 4G with various concentrations from 0–45 μg mL^{-1}, resulting in the UCNPs@ABR 4G composite. Due to FRET-induced emission quenching, the green emission of the luminescent nanoparticles gradually decreased when the amount of acceptor was increased. The relevant emission quenching mechanism can be demonstrated in Fig. 3a. The fluorescence spectra of the surface-modified UCNPs under 980 nm excitation is shown in Fig. 3b. The emission band at 520 nm and 540 nm dropped accordingly, while the 650 nm emission band almost maintained its initial intensity. Furthermore, the relationship between the intensity ratio of the green emission to red emission and the dye amount is shown in Fig. 3c. Due to the efficient FRET effect, the intensity ratio decreased when the fluorescent dye was attached to the particle surface. This intensity decay characteristic is consistent with the findings in previous literature studies,[41] which firmly indicated the FRET process in this UCNPs@ABR 4G probe under the pump. This property makes it an efficient biomarker of some target biomolecule or reactive oxygen.

3.3. Detection of hypochlorite *in vitro*

Due to the oxidizability of hypochlorite, the attached organic dye on the UCNPs surface can be oxidized and the existing FRET effect will be gradually weakened or even stopped. As a result, the quenched green emission in the previous step can be recovered. The schematic of this process is shown in Fig. 4a. Based on this emission recovery process, the relationship between the hypochlorite and upconversion emission can be established. The core–shell UCNPs modified with 30 μg mL^{-1} ABR 4G were used as a fluorescent probe during the sensing process. Here, the ClO^- with varying concentrations in the range of 0–15 ppm with a step of 3 ppm were applied as analyte. The measured fluorescence spectra under an excitation of 980 nm are shown in Fig. 5b. As the concentration of ClO^- increased from 0 ppm to 15 ppm, the green emission was found to be enhanced gradually when compared with the red emission. This emission recovery was attributed to the restrained FRET between the UCNPs and the attached organic dye. For a clear understanding of the relation between the optical signal and the analyte, the integral intensity ratio of green to red emission (IIRGRE) was extracted from the emission spectra, shown in Fig. 4c. As shown in Fig. 4c, the IIRGRE is proportional to the concentration of hypochlorite in the range from 0 to 15 ppm with a minimum detecting interval of 3 ppm. The detection limit was calculated to be 0.39 μM based on the $3\sigma/k$ method,[44] which was comparable to those reported.[16,45,46] Here, the optical response by using bare UNCPs without dye modification was also monitored as the control group, shown as the blue dots in Fig. 4c. The IIRGRE during this detection was hardly affected, which further confirmed the effectiveness of the proposed fluorescent probe in hypochlorite sensing. The gradual emission recovery picture and the relevant absorption are shown in Fig. 4d and e, where the emission intensity was dramatically enhanced and the color changed from orange to bright green. Such transformation and the gradually weakened characteristic absorption peak of ABR 4G vividly demonstrated the sensing mechanism of combination with FRET and redox. Such optical nanoprobes based on the lanthanide-doped UCNPs can be used for the highly efficient, non-invasive, stable, and real-time detection of hypochlorite, which is promising for the qualitative and quantitative monitoring of the hypochlorite level in a biological sample and water environment.

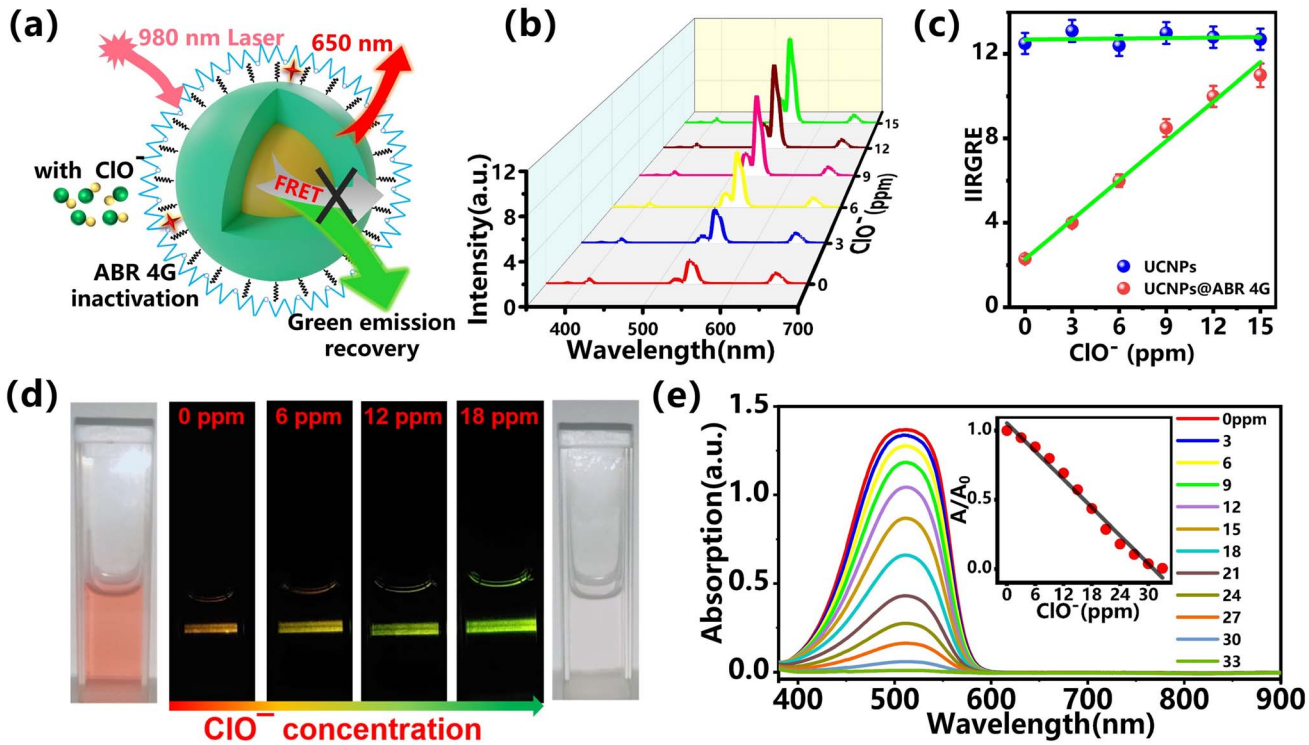

Fig. 4 (a) Diagram of ClO^- detection by UCNPs@ABR 4G; (b) the fluorescence spectrum of UCNPs@ABR 4G with different concentrations of ClO^- in the water under 980 nm near-infrared laser; (c) linear plot of the IIRGRE and the ClO^- concentration; (d) fluorescence images of the emission recovery process; (e) the absorption spectrum of UCNPs@ABR 4G with different concentrations of ClO^-; inset: the absorption ratio of UCNPs@ABR 4G with different concentrations of ClO^-.

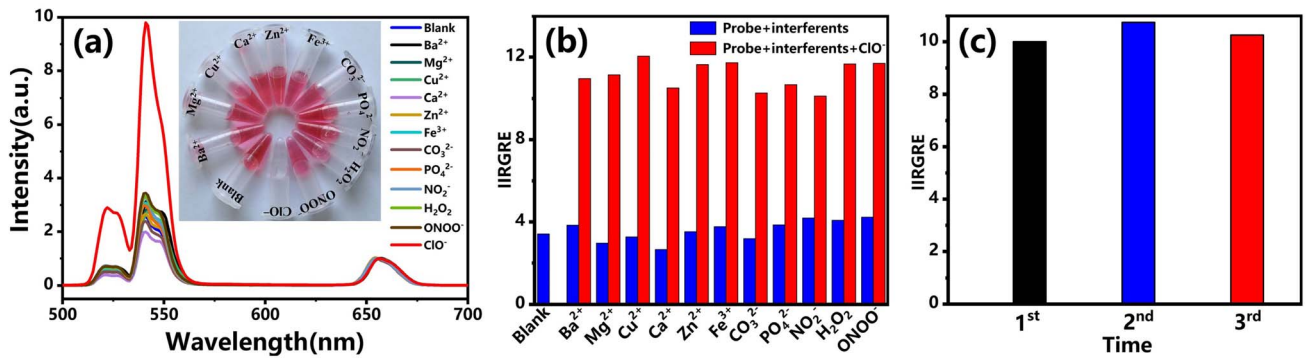

Fig. 5 (a) The fluorescence spectrum of the UCNPs@ABR 4G nanoprobe in aqueous solution: the concentration of hypochlorite was 12 ppm, the concentrations of the other ions were 76 ppm; inset: the images of the UCNPs@ABR 4G nanoprobe and other ions; (b) the IIGRGE of the UCNPs@ABR 4G nanoprobe in the absence and presence of various interferents (76 ppm), in the presence (red) and absence (blue) of ClO^- (12 ppm), respectively; (c) the IIGRGE of the UCNPs@ABR 4G nanoprobe recycled for 3 times to detect hypochlorite.

3.4. Selectivity and stability of the UCNPs@ABR 4G probe

For hypochlorite sensing, the selectivity and stability during circulation detection are two important factors for evaluating the fluorescent probe. We firstly focused on the selectivity. Here, the effects of other species such as metal ions and anions (Ca^{2+}, Mg^{2+}, Ba^{2+}, Cu^{2+}, Zn^{2+}, Fe^{3+}, NO_2^-, PO_4^{3-}, CO_3^{2-}, H_2O_2, $ONOO^-$) were considered. The emission of bare UCNPs@ABR 4G probe without anything input was used as a blank for reference. The fluorescence spectra of the UCNPs@ABR 4G nanoprobe in an aqueous solution with hypochlorite and other ions are shown in Fig. 5a. Here, the concentration of hypochlorite was 12 ppm, and the concentrations of the other ions were 76 ppm. Even though the concentrations of the other ions were much higher than that of hypochlorite, the emission recovery extended much lower than that caused by ClO^-. Further investigation of hypochlorite detection was carried out in the presence of interfering substances. After the addition of hypochlorite in those samples, the green emission was successfully recovered (Fig. 5b). For some specific environments, the ROS species are usually limited. Thus,

considering the advantages such as the large Stokes shift, stability, biocompatibility and good selectivity, the proposed upconversion probe can be qualified and effective in detecting ClO^-.

Most composite probes constructed for detecting hypochlorite, including quantum dots, fluorescent macromolecules and organic polymers, are hard to extract from the detection process and usually used as a non-recyclable reagent. However, the fluorescent probe can be recyclable due to its inorganic nanoparticle property. Here, the composite probe can be reused several times by simple centrifugal collection, and washing with water and ethanol several times. After modification by the ABR 4G molecule, it can be used to detect the hypochlorite again. Here, we select the hypochlorite with a fixed concentration of 12 ppm for detection to recycle it back and forth. Fig. 5c showed the IIRGRE for hypochlorite with a concentration of 12 ppm after three cycles, which is quite stable. These results indicated that the proposed UCNPs@ABR 4G can serve as a highly selective optical probe for the detection of ClO^- with good reusability.

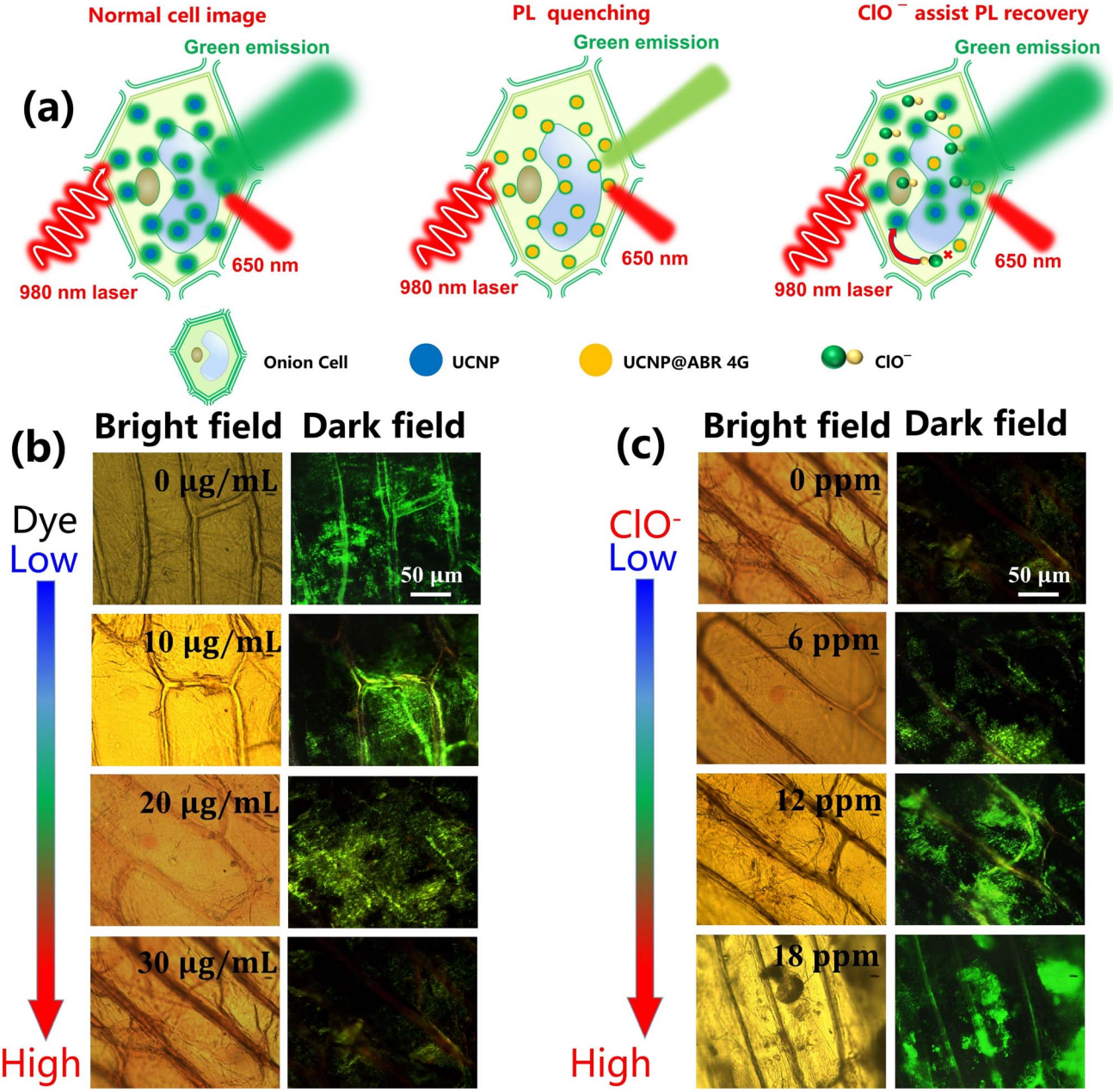

Fig. 6 (a) Schematic illustration of ClO^- detection in onion epidermal cells by using UCNP@ABR 4G nanoprobes; (b) and (c) confocal fluorescence microscopy images of onion epidermal cells incubated with UCNPs modified by ABR 4G (0, 10, 20, and 30 μg mL^{-1}, respectively), and subsequently incubated with different amounts of ClO^- (0, 6, 12, and 18 ppm, respectively). Bright field: conventional slice transmission imaging. Dark field: confocal fluorescence microscopy images of onion epidermal cells under the excitation of a 980 nm laser diode. The green channel wavelength range is 510–570 nm. Scale bar: 50 μm.

Moreover, we measured the intensity of the green emission band (510 nm–570 nm) every 4 seconds instead of continuous monitoring. It can be seen that the fluorescence intensity increased dramatically in 40 s and then leveled off. This approximate measurement also reflects the response process since the results showed similar variation with those reported in the literature,[47] as shown as Fig. S3.† The response time by using such probe was also comparable to those by using other probes within 1 minute,[47–51] and better than those over 1 minute.[47,52–54]

3.5. Monitoring and imaging of hypochlorite in the cell

The UCNPs@dye sensing system has the advantages of better biocompatibility, deep penetration of near-infrared excitation light, and low toxicity, which allows for its application to biological imaging and biosensing probes.[55] Besides the hypochlorite sensing *in vitro*, the proposed UCNPs@ABR 4G probe can also be used as a biomarker of hypochlorite in cells. Here, the fluorescence imaging technique was used for imaging and monitoring the hypochlorite in onion cells. The relevant processes are demonstrated in Fig. 6a. After incubation with UCNPs@ABR 4G for 15 min, the cells were washed and fluorescence imaging was carried out. As shown in Fig. 6b, by increasing the concentration of ABR 4G from 0 to 30 μg mL^{-1}, gradual attenuation of the comprehensive luminescence intensity in the cells with the color emission from a green color to yellow can be observed, which is consistent with the efficient energy transfer between the UCNPs and ABR 4G in the above discussion. After the hypochlorite was added, the cells gradually restored the green light emission (Fig. 6c). Here, we showed that upconversion nanoprobes are efficient and viable for imaging hypochlorite in cells based on the generation and the inhibition of the FRET process between UCNPs and ABR 4G. Such UCNPs@ ABR 4G probe and the sensing strategy will be promising for evaluating the content of hypochlorite at the subcellular levels.

The toxicity tests for the UCNPs@dye-based probe in a sensing system had been widely confirmed in previous studies.[56,57] To further reveal the cytotoxicity of this probe, herein the plasmolysis and deplasmolysis phenomena in the fluorescent probe-loaded onion cells were observed (Fig. S2†). Based on the previous report and the current results, it can be deduced that this proposed probe showed low cytotoxicity.

4. Conclusion

In summary, a hypochlorite detection approach based on the ABR 4G-modified $NaGdF_4$:Yb^{3+}, Er^{3+}@$NaYF_4$ upconversion probe was developed in this work. We found that the IIRGRE of UCNPs@ABR 4G was sensitive to the concentration of hypochlorite, and the relationship between the analyte concentration and the signal intensity was linear. By eliminating the amount of emission quencher and inhibiting the FRET effect, the UCNPs green emission can be recovered with the existence of hypochlorite. The proposed fluorescent probe was also used for the detection and imaging of hypochlorite in aqueous solution and living cells. Such a strategy possesses the superiority of high selectivity and stability, non-invasiveness, biocompatibility and quick response, which provides a new option for the detection of hypochlorite in microenvironments.

Conflicts of interest

The authors declare that they have no known competing financial interests or personal relationships that could have appeared to influence the work reported in this paper.

Acknowledgements

This work was funded by the National Natural Science Foundations of China (Grant No. 61905075, 62173135 and 62175062), and Scientific Research Fund of Hunan Provincial Education Department (under Grant No. 20A1933).

References

1 Y. Ren, S. Liu, L. Yang, *et al.*, Practice and exploration of infection prevention and control measures based on risk management of surgical patients during the epidemic of corona virus disease 2019 (COVID-19), *Am. J. Infect. Control*, 2021, **49**(2), 151–157.
2 S. W. K. Tang, M. R. Romano, D. H. T. Wong, *et al.*, The use of personal protective equipment in clinical ophthalmology during corona virus disease-2019: a review of international guidelines and literature, *Curr. Opin. Ophthalmol.*, 2020, **31**(5), 435–446.
3 Y. Hu, J. Sun, Z. Dai, *et al.*, Prevalence and severity of corona virus disease 2019 (COVID-19): A systematic review and meta-analysis, *J. Clin. Virol.*, 2020, **127**, 104371.
4 R. F. Sharaf and N. Kabel, Awareness and knowledge of undergraduate dental students about the signs and symptoms of Corona viral infection (COVID-19), and the required infection control measures to prevent its spread, *Bull. Natl. Res. Cent.*, 2021, **45**(1), 1–9.
5 A. Chatterjee, Use of hypochlorite solution as disinfectant during COVID-19 outbreak in India: from the perspective of human health and atmospheric chemistry, *Aerosol Air Qual. Res.*, 2020, **20**(7), 1516–1519.
6 D. Wu, L. Chen, Q. Xu, *et al.*, Design principles, sensing mechanisms, and applications of highly specific fluorescent probes for HOCl/OCl, *Acc. Chem. Res.*, 2019, **52**(8), 2158–2168.
7 L. Long, Y. Han, W. Liu, *et al.*, Simultaneous discrimination of hypochlorite and single oxygen during sepsis by a dual-functional fluorescent probe, *Anal. Chem.*, 2020, **92**(8), 6072–6080.
8 N. Zhu, X. Guo, S. Pang, *et al.*, Mitochondria-immobilized unimolecular fluorescent probe for multiplexing imaging of living cancer cells, *Anal. Chem.*, 2020, **92**(16), 11103–11110.
9 A. Ulfig and L. I. Leichert, The effects of neutrophil-generated hypochlorous acid and other hypohalous acids on host and pathogens, *Cell. Mol. Life Sci.*, 2021, **78**(2), 385–414.

10 X. He, Z. Deng, W. Xu, *et al.*, A novel dual-response chemosensor for bioimaging of Exogenous/Endogenous hypochlorite and hydrazine in living cells, Pseudomonas aeruginosa and zebrafish, *Sens. Actuators, B*, 2020, **321**, 128450.

11 C. Xu, Y. Zhou, Z. Li, *et al.*, Rational design of AIE-based fluorescent probes for hypochlorite detection in real water samples and live cell imaging, *J. Hazard. Mater.*, 2021, **418**, 126243.

12 Y. Zhu, Y. Ma, Y. Liu, *et al.*, Fluorescence response of a fluorescein derivative for hypochlorite ion and its application for biological imaging in wounded zebrafish and living mice, *Sens. Actuators, B*, 2021, **327**, 128848.

13 N. Kwon, D. Kim, K. M. K. Swamy, *et al.*, Metal-coordinated fluorescent and luminescent probes for reactive oxygen species (ROS) and reactive nitrogen species (RNS), *Coord. Chem. Rev.*, 2021, **427**, 213581.

14 J. Haginaka and J. Wakai, Liquid chromatographic determination of amoxicillin and its metabolites in human urine by postcolumn degradation with sodium hypochlorite, *J. Chromatogr. B: Biomed. Sci. Appl.*, 1987, **413**, 219–226.

15 C. Zetterberg and T. Öfverholm, Carpal tunnel syndrome and other wrist/hand symptoms and signs in male and female car assembly workers, *Int. J. Ind. Ergon.*, 1999, **23**(3), 193–204.

16 L. Wonjung, H. Youn, J. Bae, *et al.*, Solid-phase colorimetric sensor for hypochlorite, *Analyst*, 2021, **146**(7), 2301–2306.

17 L. Lu, J. Zhang and X. Yang, Simple and selective colorimetric detection of hypochlorite based on anti-aggregation of gold nanoparticles, *Sens. Actuators, B*, 2013, **184**, 189–195.

18 R. T. Emmet, Spectrophotometric determination of urea and ammonia in natural waters with hypochlorite and phenol, *Anal. Chem.*, 1969, **41**(12), 1648–1652.

19 E. Vidal, A. S. Lorenzetti, C. D. Garcia, *et al.*, Use of universal 3D-Printed smartphone spectrophotometer to develop a time-based analysis for hypochlorite, *Anal. Chim. Acta*, 2021, **1151**, 338249.

20 J. M. Mohan, K. Amreen, A. Javed, *et al.*, Miniaturized 3D printed electrochemical platform with optimized Fibrous carbon electrode for non-interfering hypochlorite sensing, *Chemosphere*, 2022, 134915.

21 D. R. Kumar, S. Kesavan, T. T. Nguyen, *et al.*, Polydopamine@ electrochemically reduced graphene oxide-modified electrode for electrochemical detection of free-chlorine, *Sens. Actuators, B*, 2017, **240**, 818–828.

22 B. Zhu, W. Tang, Y. Ren, *et al.*, Chemiluminescence of conjugated-polymer nanoparticles by direct oxidation with hypochlorite, *Anal. Chem.*, 2018, **90**(22), 13714–13722.

23 J. Li and P. K. Dasgupta, Chemiluminescence detection with a liquid core waveguide: determination of ammonium with electrogenerated hypochlorite based on the luminol-hypochlorite reaction, *Anal. Chim. Acta*, 1999, **398**(1), 33–39.

24 N. Zhao, Y. H. Wu, R. M. Wang, *et al.*, An iridium (iii) complex of oximated 2, 2′-bipyridine as a sensitive phosphorescent sensor for hypochlorite, *Analyst*, 2011, **136**(11), 2277–2282.

25 R. Zhang, Z. Ye, B. Song, *et al.*, Development of a ruthenium (II) complex-based luminescent probe for hypochlorous acid in living cells, *Inorg. Chem.*, 2013, **52**(18), 10325–10331.

26 Z. Lu, M. Shangguan, X. Jiang, *et al.*, A water-soluble cyclometalated iridium (III) complex with fluorescent sensing capability for hypochlorite, *Dyes Pigm.*, 2019, **171**, 107715.

27 H. Li, H. Kim, F. Xu, *et al.*, Activity-based NIR fluorescent probes based on the versatile hemicyanine scaffold: design strategy, biomedical applications, and outlook, *Chem. Soc. Rev.*, 2022, **51**, 1795–1835.

28 S. I. Reja, I. A. Khan, V. Bhalla, *et al.*, A TICT based NIR-fluorescent probe for human serum albumin: a pre-clinical diagnosis in blood serum, *Chem. Commun.*, 2016, **52**(6), 1182–1185.

29 T. B. Ren, Z. Y. Wang, Z. Xiang, *et al.*, A General Strategy for Development of Activatable NIR-II Fluorescent Probes for *In Vivo* High-Contrast Bioimaging, *Angew. Chem.*, 2021, **133**(2), 813–818.

30 M. Lin, Y. Zhao, S. Q. Wang, *et al.*, Recent advances in synthesis and surface modification of lanthanide-doped upconversion nanoparticles for biomedical applications, *Biotechnol. Adv.*, 2012, **30**(6), 1551–1561.

31 S. Wen, J. Zhou, K. Zheng, *et al.*, Advances in highly doped upconversion nanoparticles, *Nat. Commun.*, 2018, **9**(1), 1–12.

32 S. Borse, R. Rafique, Z. V. P. Murthy, *et al.*, Applications of upconversion nanoparticles in analytical and biomedical sciences: A review, *Analyst*, 2022, **147**, 3155–3179.

33 F. Wang, D. Banerjee, Y. Liu, *et al.*, Upconversion nanoparticles in biological labeling, imaging, and therapy, *Analyst*, 2010, **135**(8), 1839–1854.

34 L. Zhang, D. Jin and M. H. Stenzel, Polymer-functionalized upconversion nanoparticles for light/imaging-guided drug delivery, *Biomacromolecules*, 2021, **22**(8), 3168–3201.

35 R. Xu, H. Cao, D. Lin, *et al.*, Lanthanide-doped upconversion nanoparticles for biological super-resolution fluorescence imaging, *Cell Rep. Phys. Sci.*, 2022, 100922.

36 S. Zhan, J. Xiong, G. Nie, S. Wu, J. Hu, X. Wu, S. Hu, J. Zhang, Y. Gao and Y. Liu, *Adv. Mater. Interfaces*, 2019, **6**, 1802089.

37 Y. Liu, J. Vanacken, X. Chen, J. Han, Z. Zhong, Z. Xia, B. Chen, H. Wu, Z. Jin, J. Ge, J. Huang, L. Meng, X. Duan, Y. Huang, Q. Peng, V. Moshchalkov and Y. Li, *Adv. Mater.*, 2019, **31**, 1806341.

38 X. Wu, S. Zhan, J. Han, *et al.*, Nanoscale ultrasensitive temperature sensing based on upconversion nanoparticles with lattice self-adaptation, *Nano Lett.*, 2020, **21**(1), 272–278.

39 G. Huang, X. Wu, S. Zhan, *et al.*, Simultaneous enhancement of fluorescence intensity, thermometric sensitivity and SNR of upconversion thermometers *via* optical field localization, *J. Mater. Chem. C*, 2022, **10**(13), 5190–5199.

40 Y. Liu, D. Wang, J. Shi, *et al.*, Magnetic tuning of upconversion luminescence in lanthanide-doped bifunctional nanocrystals, *Angew. Chem.*, 2013, **125**(16), 4462–4465.

41 A. A. Ansari, V. K. Thakur and G. Chen, Functionalized upconversion nanoparticles: New strategy towards FRET-based luminescence bio-sensing, *Coord. Chem. Rev.*, 2021, **436**, 213821.

42 L. Liu, H. Zhang, Z. Wang, *et al.*, Peptide-functionalized upconversion nanoparticles-based FRET sensing platform for Caspase-9 activity detection *in vitro* and *in vivo*, *Biosens. Bioelectron.*, 2019, **141**, 111403.

43 L. Yuan, W. Lin, K. Zheng, *et al.*, FRET-based small-molecule fluorescent probes: rational design and bioimaging applications, *Acc. Chem. Res.*, 2013, **46**(7), 1462–1473.

44 C. Xu, Y. Zhou, Z. Li, *et al.*, Rational design of AIE-based fluorescent probes for hypochlorite detection in real water samples and live cell imaging, *J. Hazard. Mater.*, 2021, **418**, 126243.

45 X. Kong, S. M. Shuang, Y. Zhang, *et al.*, Dicyanoisophorone-based fluorescent probe with large Stokes shift for ratiometric detection and imaging of exogenous/endogenous hypochlorite in cell and zebrafish, *Talanta*, 2022, **242**, 123293.

46 H. Yin, H. Chi, Z. Shang, *et al.*, Development of a new water-soluble fluorescence probe for hypochlorous acid detection in drinking water, *Food Chem.: Mol. Sci.*, 2021, **2**, 100027.

47 Y. Zhang, L. Ma, C. Tang, *et al.*, A highly sensitive and rapidly responding fluorescent probe based on a rhodol fluorophore for imaging endogenous hypochlorite in living mice, *J. Mater. Chem. B*, 2018, **6**(5), 725–731.

48 C. Zhang, X. Li, Y. Jiang, *et al.*, A super large Stokes shift ratiometric fluorescent probe for highly selective sensing of ClO^- in bio-imaging and real water samples, *Spectrochim. Acta, Part A*, 2022, **283**, 121736.

49 Y. Zhang, L. Ma, C. Tang, *et al.*, A highly sensitive and rapidly responding fluorescent probe based on a rhodol fluorophore for imaging endogenous hypochlorite in living mice, *J. Mater. Chem. B*, 2018, **6**(5), 725–731.

50 Q. Fu, G. Chen, Y. Liu, *et al.*, *In situ* quantification and evaluation of ClO^-/H 2 S homeostasis in inflammatory gastric tissue by applying a rationally designed dual-response fluorescence probe featuring a novel H+-activated mechanism, *Analyst*, 2017, **142**(9), 1619–1627.

51 Y. N. Zeng, H. Q. Zheng, X. H. He, *et al.*, Dual-emissive metal–organic framework: a novel turn-on and ratiometric fluorescent sensor for highly efficient and specific detection of hypochlorite, *Dalton Trans.*, 2020, **49**(28), 9680–9687.

52 K. Zhang, H. Wang, S. Cheng, *et al.*, A benzaldehyde–indole fused chromophore-based fluorescent probe for double-response to cyanide and hypochlorite in living cells, *Analyst*, 2021, **146**(18), 5658–5667.

53 Y. Shen, C. Nie, C. Zhu, *et al.*, Aggregation-Induced Emission Fluorophore-Incorporated Curcumin-Based Ratiometric Nanoprobe for Hypochlorite Detection in Food Matrices, *J. Agric. Food Chem.*, 2022, **70**(30), 9577–9583.

54 J. Fan, H. Mu, H. Zhu, *et al.*, Light up ClO^- in live cells using an aza-coumarin based fluorescent probe with fast response and high sensitivity, *Analyst*, 2015, **140**(13), 4594–4598.

55 M. Wang, R. Mi, L. Wang, *et al.*, Preparation of cyanine dye sensitized upconversion luminescent nanoprobe and hypochlorous acid detection by light-emitting energy transfer, *J. Lumin.*, 2021, **239**, 118395.

56 Z. Chen, X. Wu, S. Hu, *et al.*, Upconversion NaLuF 4 fluorescent nanoprobes for jellyfish cell imaging and irritation assessment of organic dyes, *J. Mater. Chem. C*, 2015, **3**(23), 6067–6076.

57 Z. Chen, X. Wu, S. Hu, *et al.*, Upconversion fluorescent and X-ray-sensitive bifunctional nanoprobes for assessing the penetrability of inorganic nanoparticles in the digestive system, *MedChemComm*, 2017, **8**(5), 1053–1062.